AGU PUBLICATIONS

JGR

Journal of Geophysical Research: Space Physics

RESEARCH ARTICLE
10.1002/2015JA022077

Special Section:
Inner Magnetosphere Coupling: Recent Advances

Structure and evolution of electron "zebra stripes" in the inner radiation belt

Y. Liu[1], Q.-G. Zong[1], X.-Z. Zhou[1], J. C. Foster[2], and R. Rankin[3]

[1]Institute of Space Physics and Applied Technology, Peking University, Beijing, China, [2]Haystack Observatory, Massachusetts Institute of Technology, Westford, Massachusetts, USA, [3]Department of Physics, University of Alberta, Edmonton, Alberta, Canada

Key Points:
- Zebra stripes are evenly spaced patterns in electron drift coordinate
- Zebra stripes evolves in proportion to real time
- Zebra stripes are produced by electron motion under static/single monochromatic electric field

Correspondence to:
Q.-G. Zong,
qgzong@pku.edu.cn

Citation:
Liu Y., Q.-G. Zong, X.-Z. Zhou, J. C. Foster, and R. Rankin (2016), Structure and evolution of electron "zebra stripes" in the inner radiation belt, *J. Geophys. Res. Space Physics*, *121*, 4145–4157, doi:10.1002/2015JA022077.

Received 25 OCT 2015
Accepted 5 APR 2016
Accepted article online 11 APR 2016
Published online 10 MAY 2016

Abstract "Zebra stripes" are newly found energetic electron energy-spatial (L shell) distributed structure with an energy between tens to a few hundreds keV in the inner radiation belt. Using high-quality measurements of electron fluxes from Radiation Belt Storm Probes Ion Composition Experiment (RBSPICE) on board the twin Van Allen Probes, we carry out case and statistical studies from April 2013 to April 2014 to study the structural and evolutionary characteristics of zebra stripes below $L = 3$. It is revealed that the zebra stripes can be transformed into evenly spaced patterns in the electron drift frequency coordinate: the detrended logarithmic fluxes in each L shell region can be well described by sinusoidal functions of drift frequency. The "wave number" of this sinusoidal function, which corresponds to the reciprocal of the gap between two adjacent peaks in the drift frequency coordinate, increases in proportion to real time. Further, these structural and evolutionary characteristics of zebra stripes can be reproduced by an analytic model of the evolution of the particle distribution under a single monochromatic or static azimuthal electric field. It is shown that the essential ingredient for the formation of multiple zebra stripes is the periodic drift of particles. The amplitude of the zebra stripes shows a good positive correlation with *Kp* index, which indicates that the generation mechanism of zebra stripes should be related to geomagnetic activities.

1. Introduction

In the inner radiation belt, the energy spectra of energetic electrons have long been reported to have one or multiple peaks. Such a peak was first reported by *Imhof and Smith* [1966], who have identified a single peak at the energy of 1.3 MeV. *Cladis* [1966] developed a model of electron acceleration by drift resonance to understand the generation of such peaks. Later on, multiple peaks in the spectrum from 68 to 1152 keV were detected by P78-1 satellite and reported by *Imhof et al.* [1981]. These peaks were found to have a nearly constant drift period over a broad range of L shells. By using S81-1 observations, *Datlowe et al.* [1985] further suggested that multiple peaks in the energetic electron spectra were observed on most days in all levels of geomagnetic activity.

Recently, observations from the Demeter satellite [*Sauvaud et al.*, 2013] and Van Allen Probes [*Ukhorskiy et al.*, 2014] have shown that such peaks in electron energy spectrogram are organized in regular patterns across the entire inner radiation belt. *Sauvaud et al.* [2013] found that these regular patterns are along constant drift periods. Their statistical analysis showed that the occurrence rate of the fine structures correlates with geomagnetic activities, and they argued that these structures are caused by resonant interaction of energetic electrons with ultralow frequency (ULF) waves associated with enhanced solar wind driving. In order to create multiple patterns by this resonance mechanism, the perturbations must be composed of multiple wave modes with discrete spatial structures.

The newly launched Van Allen Probes are designed to explore the dynamics of energetic charged particles [*Mauk et al.*, 2012] with higher temporal and energy resolutions. Based on Van Allen Probe observations, *Ukhorskiy et al.* [2014] found that regular patterns in the electron spectrogram are ubiquitous features in the inner radiation belt and named them "zebra stripes." They pointed out that ULF waves are not long-lasting, and they typically do not exhibit discrete spatial structures. By using a test-particle model, they found that these stripes can be produced by a global monochromatic azimuthal electric field. They suggested that the proposed monochromatic electric field originates from the diurnal oscillations of corotation region to the outer magnetosphere.

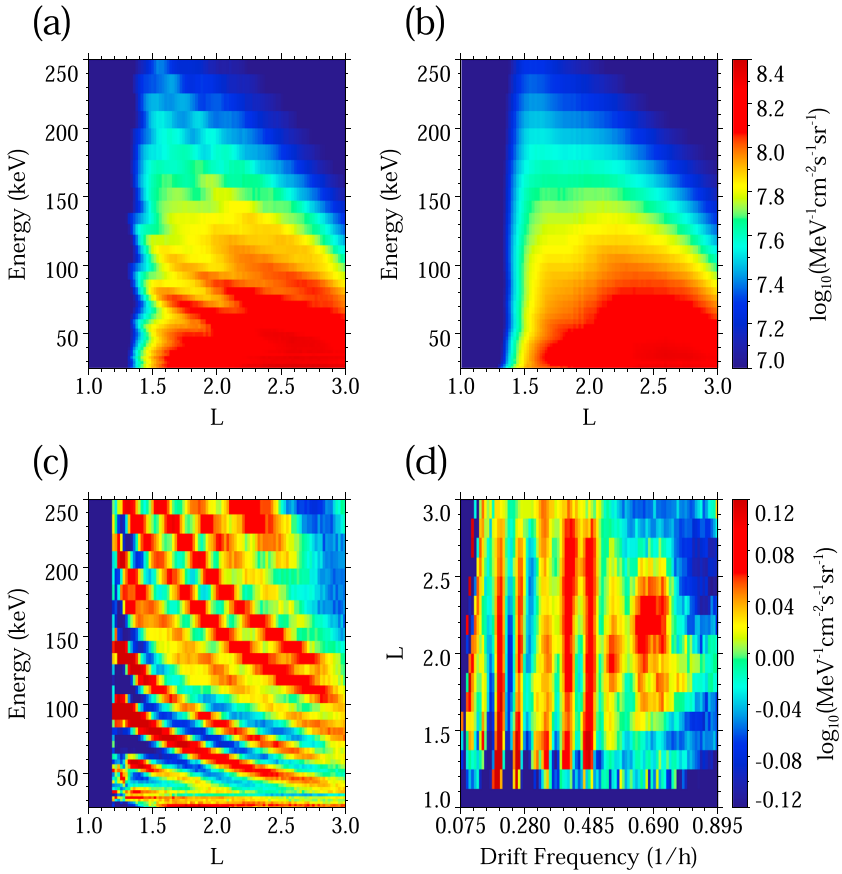

Figure 1. Energetic electron spectrogram for a pass of VAP A on 20 December 2013. (a) Energy-*L* spectrogram of logarithmic electron fluxes in the energy range 25 keV to 250 keV and L shell range 1–3. (b) Smoothed logarithmic electron flux spectrogram with same format as Figure 1a. (c) Detrended logarithmic electron flux spectrum with same format as Figure 1a. (d) $L - f_d$ spectrogram of detrended logarithmic electron fluxes in the L shell range 1–3.

In this paper, we further analyze the electron measurements from Van Allen Probes to reveal the features of zebra stripes inside $L = 3$. A quantitative and comprehensive analysis on the structure and evolution of zebra stripes have been carried out based on continuous measurements for the first time. To interpret the exact features obtained in the observations, an analytical model of the evolution of the particle distribution under a single monochromatic/static azimuthal electric field is developed. Our analytic model is a quantification and generalization of the test particle model developed by *Ukhorskiy et al.* [2014]. Our analytic model will show that either a static or a monochromatic electric field can produce the observed zebra stripes by Van Allen Probes.

2. Observations

2.1. Data and Methodology

Since launched in 2012, the NASA's twin Van Allen Probes (VAPs) have provided continuous measurements of Earth's radiation belts in a highly elliptical, low inclination orbit [*Mauk et al.*, 2012]. The data sets we used in our study are taken from the Radiation Belt Storm Probes Ion Composition Experiment (RBSPICE) [*Mitchell et al.*, 2013], which measures energetic electrons from about 25 keV to 1 MeV. The high-energy resolution data we used have 64 energy channels, which provide a great opportunity to investigate fine structures in the electron spectrum of the inner radiation belt.

In this study, we focus on energetic electrons with equatorial pitch angles between 60 and 120°. More specifically, we use TS04 model [*Tsyganenko and Sitnov*, 2005] to transform in situ pitch angles to equatorial pitch angles, and the average of fluxes is taken among telescopes within the equatorial pitch angle range between 60 and 120°.

2.2. Case Study: Single Observation on 20 December 2013

Figure 1 presents the electron spectrograms taken during a pass of VAP A from $L \approx 3$ at 17:11:23 UT to the perigee at 18:05:07 UT on 20 December 2013. Figure 1a displays the energy-L spectrogram of logarithmic electron fluxes in the energy range from 25 to 250 keV and L shell from 1 to 3. As we can see, the energetic electrons are well organized in regular patterns referred to as zebra stripes in *Ukhorskiy et al.* [2014]. To better illustrate the characteristics of the patterns, we first compute at each L location the nine-energy-channel sliding average of the logarithmic electron fluxes (shown in Figure 1b) and then derive the detrended logarithmic fluxes (Figure 1c) by subtracting the smoothed logarithmic fluxes from original logarithmic fluxes. For the sake of showing more essential features, we next calculate the drift frequency of energetic electrons using the following formula (developed in a dipole field based on the formula in *Roederer* [1970]):

$$f_d = \frac{3m_0c^2\beta^2\gamma L}{4\pi eB_0R_E^2} + f_{\text{cor}} \tag{1}$$

where $\beta = v/c$ is the relativistic velocity factor, γ is the relativistic energy factor, R_E is the radius of the Earth, B_0=3.11 × 10^5 nT is the magnitude of magnetic field at magnetic equator, L is the L shell parameter, and f_{cor}=1 day^{-1} is the frequency of the plasma corotation. Detrended logarithmic fluxes in Figure 1c are then rearranged into $L - f_d$ coordinate, as shown in Figure 1d. In this figure, the "stripes" are presented as nearly evenly spaced vertical patterns. This reveals that the stripes are one-dimensional structure in the drift frequency space.

To quantitatively analyze the features of zebra stripes, we divide data into three L shell regions (1.5–2.0, 2.0–2.5, and 2.5–3.0). In each region, the electron flux J and the detrended logarithmic flux are obtained as the functions of drift frequency. The detrended logarithmic flux is defined as $\log(J) - \overline{\log(J)}$, where $\overline{\log(J)}$ is a sliding average of $\log(J)$ in drift frequency coordinate. Figure 2 displays the analysis results of the same observation as in Figure 1. Figures 2a–2c show the results of three L shell regions (1.5–2.0, 2.0–2.5, and 2.5–3.0), respectively. In each sub-figure, the upper-left panel shows the flux as a function of electron drift frequency, and the bottom-left panel shows the corresponding detrended logarithmic flux. The data between the two dashed red lines, which represent the 15%–65% of the drift frequency range, are then selected to perform Fourier analysis; the resulting power spectral density profiles is shown in the right panel.

In Figure 2, the detrended logarithmic fluxes in the selected drift frequency range present sine-like structures in all three L shell regions. Furthermore, the wave lengths and phases of these structures are nearly the same among these L shell regions. The power spectral density profiles also show a remarkable peak at the same wave length. To achieve a more quantitative result, we use the following formula to fit the detrended logarithmic fluxes in the selected frequency range:

$$p = A\sin(2\pi T f_d - \phi_0) \tag{2}$$

where p is the detrended logarithmic flux, A is the amplitude of the sinusoidal function, f_d is the drift frequency, ϕ_0 is the phase angle, and T is a time quantity which we name "evolution time." The parameter T can be understood as the wave number of the structures in the detrended logarithmic fluxes. Large T corresponds to denser stripes while small T corresponds to sparse stripes.

In the best fit procedure, we define A as the square root of the peak power spectral density and then determine T and ϕ_0 on a least squares basis. The fitting results are presented as blue lines in Figure 2. The T and ϕ_0 values, in the three L shell regions (1.5–2.0, 2.0–2.5, and 2.5–3.0), are 13.6, 13.5, and 13.5, and 2.2, 2.1, and 2.2, respectively. To evaluate best fit quality, we calculate for each fitting the R^2 value defined as

$$R^2 = 1 - \frac{\sum_i (p_i - \hat{p}_i)^2}{\sum_i (p_i - \overline{p})^2} \tag{3}$$

where p_i is the observed data, $\hat{p}_i$ is the modeled value associated with p_i, $\overline{p}$ is the average of observed data. It is obvious that the larger R^2 is, the better the model fits the observed data. The resulting R^2 values are 0.63, 0.72, and 0.61 in the three L shell regions (1.5–2.0, 2.0–2.5, and 2.5–3.0), respectively, which indicate that the detrended logarithmic fluxes can be well described by sinusoidal functions.

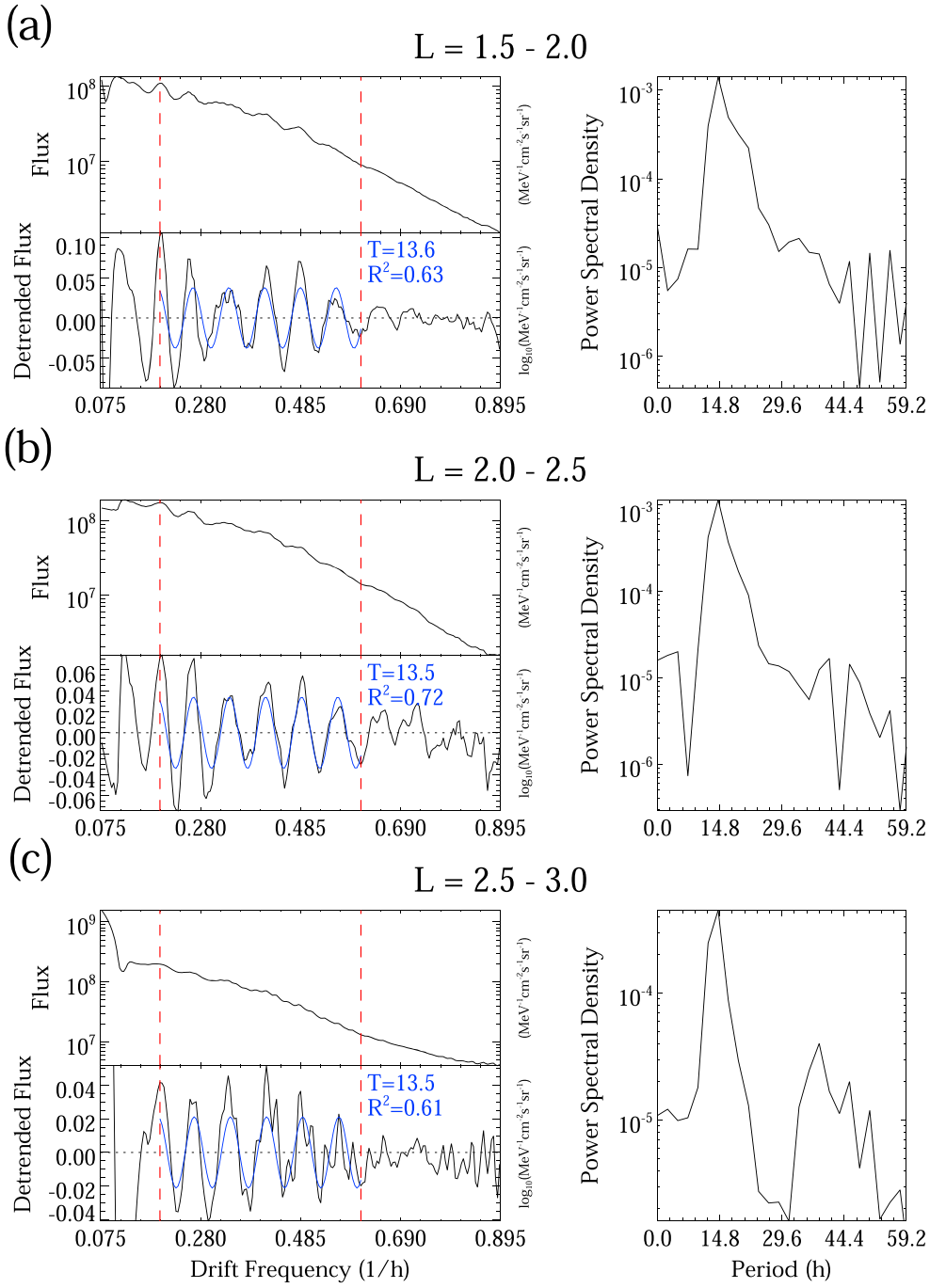

Figure 2. Energetic electron flux versus drift frequency observed by VAP A on 20 December 2013. (a–c) Results in three L shell regions (1.5–2.0, 2.0–2.5, and 2.5–3.0), respectively. In each subfigure, the black line in the upper left (bottom left) represents the flux (detrended logarithmic flux) as a function of drift frequency, while the blue line in the bottom left represents the fitted detrended logarithmic flux. The right column represents the power spectral density of the detrended logarithmic fluxes between the two dashed red lines.

In summary for this section, we show that in this event, the zebra stripes are arranged periodically in the drift frequency coordinate. The detrended logarithmic fluxes in the three L shell regions (1.5–2.0, 2.0–2.5, and 2.5–3.0) can all be approximated by sine-like functions with nearly same period and phase angle. By fitting the fluxes with a sinusoidal function, the evolution time T, phase angle ϕ_0 and fit goodness R^2 are obtained. These parameters will be used in the next sections to describe the characteristics of zebra stripes.

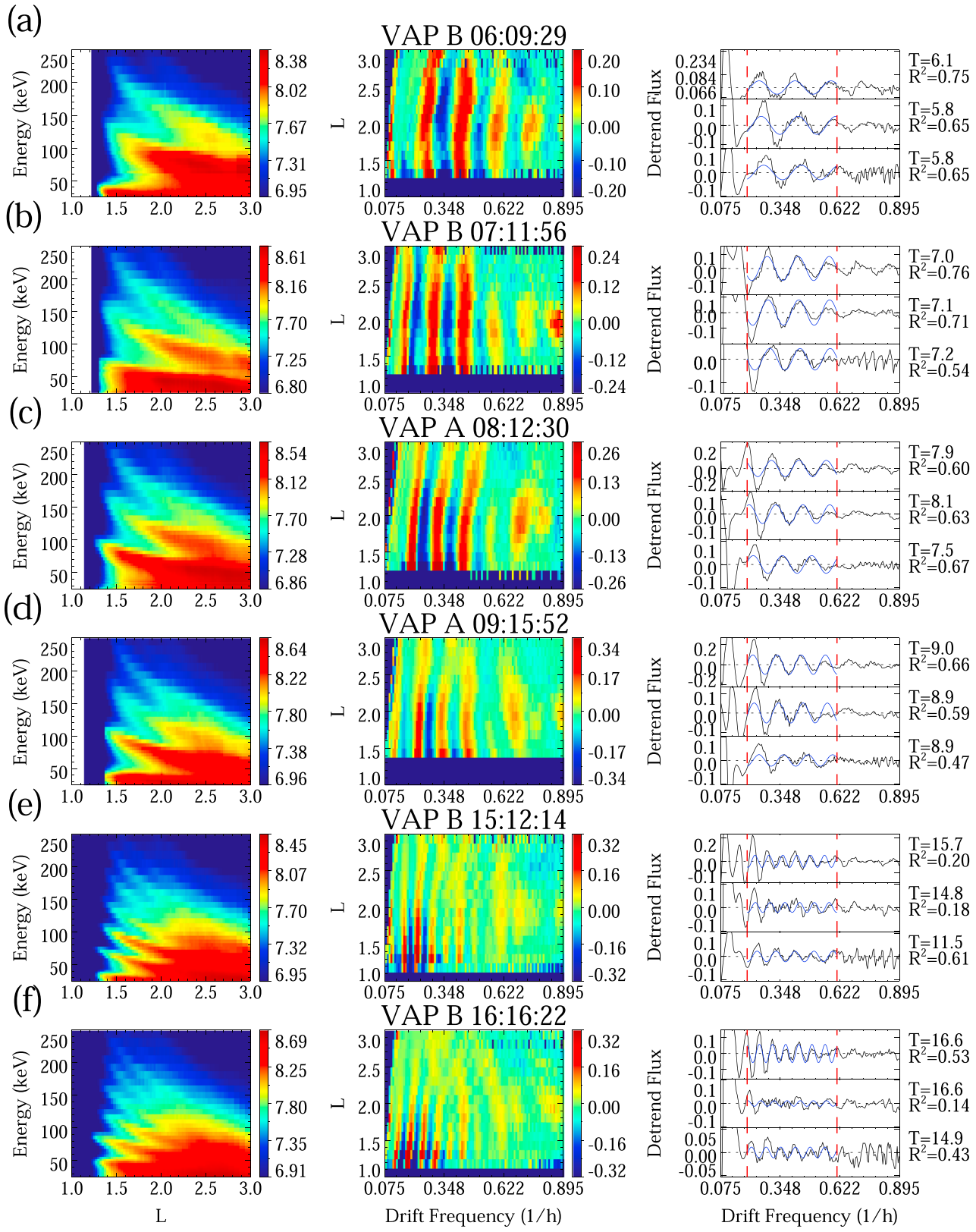

Figure 3. Continuous electron spectrograms observed by VAPs on 16 February 2014. (left column) Energy-L spectrogram of energetic electrons. (middle column) $L - f_d$ spectrogram of detrended logarithmic energetic electrons as Figure 1. (right column) detrended logarithmic fluxes (black lines) and fitted detrended logarithmic fluxes (blue lines) in three L shell regions (1.5–2.0, 2.0–2.5, and 2.5–3.0), respectively, as Figure 2.

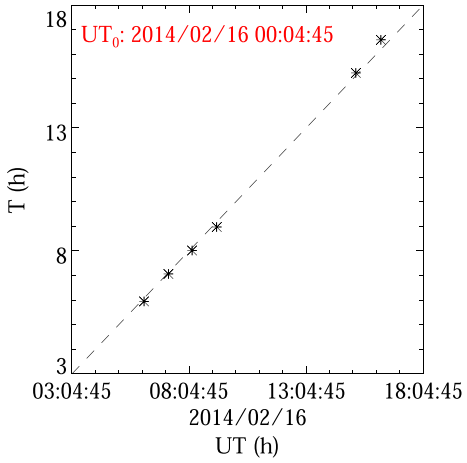

Figure 4. The relationship between averaged evolution time and satellite epoch at $L=2$ on 16 February 2014. The star points represent six single observations in Figure 3, and the dashed line represents $T = UT - UT_0$.

2.3. Case Study: Continuous Observations on 16 February 2014

In this section, we present a case with continuous observations of zebra stripes by both VAP A and VAP B. On 16 February 2014, VAP A and VAP B went through L shell 1–3 several times and show continuous evolution of zebra stripes. Since each electron spectrogram is measured over a sustained period of time, we simply use the time when satellite arrive at $L=2$ as the observation time of the corresponding electron spectrogram. Under this definition, on 16 February 2014 VAP B first observed the zebra stripes at 06:09:29 UT and 07:11:56 UT, and then VAP A observed the zebra stripes at 08:12:30 UT and 09:15:52 UT. Finally, VAP B observed the zebra stripes again at 15:12:14 UT and 16:16:22 UT.

The six continuous observations of the electron spectrograms and the corresponding analysis results are displayed in Figure 3. Figures 3a–3f show the six observations in chronological order. Figures 3a (left) to 3f (left) are the energy-L spectrograms of electron flux, and Figures 3a (middle) to 3f (middle) are the $L - f_d$ spectrograms of detrended logarithmic flux in the same format as in Figures 1a and 1d. Figures 3a (right) to 3f (right) present the detrended logarithmic fluxes in the three L shell regions (1.5–2.0, 2.0–2.5, and 2.5–3.0) with the same format in Figure 2.

As shown in Figure 3, the six electron spectrograms are all organized in evenly spaced, nearly vertical patterns in the $L - f_d$ coordinate. It is noted that the patterns may have small slopes, which probably arises from the different observation times at different L shells. Figures 3a (right) to 3f (right) show that the detrended logarithmic fluxes are presented as sine-like curves in all the three L shell regions. The best fit results agree with the observations in general; except that in Figure 3e and Figure 3f, the fitting is less successful due to the limited energy resolution of the satellite measurements. From these results one can find that the periods and phase angles of the fitted sinusoidal functions hardly depend on L. Moreover, the stripes become denser (indicated by the increasing T values) as time progresses.

We next show the relationship between the evolution time T and the real time. Here we use the averaged T of L shell regions 1.5–2.0 and 2.0–2.5 as the evolution time of each snapshot, and its comparison with real time is given in Figure 4. The evolution time T of L shell region 2.5– 3.0 is not used because the energy resolution is not enough to identify the zebra stripes in this region when T is large. In Figure 4, each star point represents one single observation in Figure 3, and the dashed line represents $T = UT - UT_0$. The star points are all nearly located in the dashed line, which means the structure parameter T are closely associated with the real time. Therefore, we speculate that the evolution time may be interpreted as the time it takes for the zebra stripes to evolve into current state.

2.4. Statistical Study

In this section, we use statistical study to verify the structural and evolutionary features implied in the two case studies. Continuous data of the two VAPs from April 2013 to April 2014 are analyzed in this section. For each single observation in L shell range 1–3, we divide the electron flux data into three L shell regions and fit the detrended logarithmic fluxes by the sinusoidal functions as described in section 2.1. The derived parameters A, T, ϕ_0, and R^2 are used for statistical analysis below.

Figure 5 displays the distribution of coefficient of determination R^2 and the relationship between amplitude A and R^2. Figure 5 (left) to 5 (right) show the results in three L shell regions (1.5–2.0, 2.0–2.5, and 2.5–3.0), respectively. As shown in this figure, R^2 is larger than 0.3 for over half of the single observations in the L shell region 1.5–2.0 and 2.0–2.5. In L shell region 2.5–3.0, the R^2 is smaller generally, which may be due to the limited energy resolution of the satellite measurements and smaller amplitude of zebra stripes. Further, this figure shows a good positive correlation between A and R^2. Since the amplitude A is derived from the power

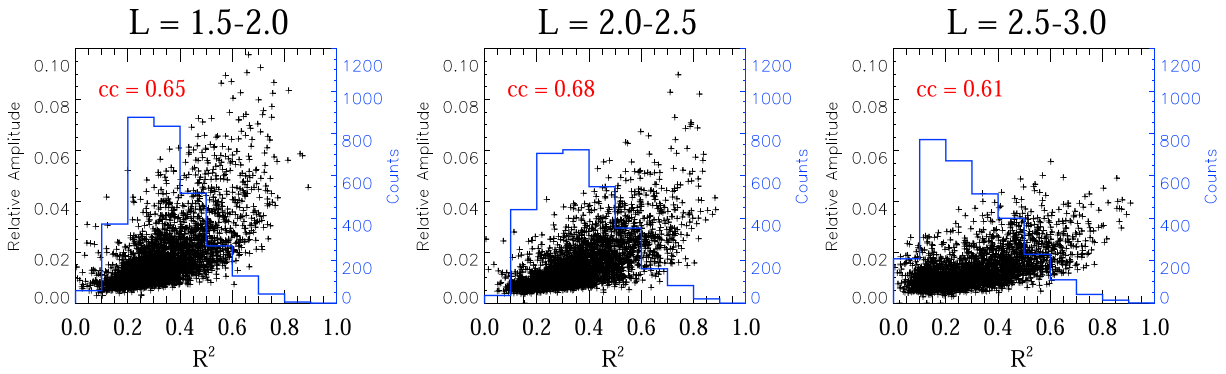

Figure 5. Distribution of the R^2 value and the relationship between the relative amplitude A and R^2 in three L shell regions (1.5–2.0, 2.0–2.5, and 2.5–3.0). The histogram shows the number of cases at each R^2 value bin. Each black cross point represents parameters from one single observation. The parameter "cc" represents the linear correlation coefficient between A and R^2.

spectral density of the detrended logarithmic fluxes, it can reflect the intensity of the disturbance superposed in the smoothed electron spectrum. When A is small, there are no regular patterns, or at most shallow patterns mixed with random perturbations and measurement errors. When A is large, clear regular patterns can be seen in the electron spectrograms, and they can be fitted well by the sinusoidal function. This statistical result indicates that the zebra stripes (manifest as evenly spaced structures in the drift frequency coordinate) is an ubiquitous feature of electrons in the inner radiation belt.

Figure 6 displays the comparison of phase angles ϕ_0 between L shell regions 1.5–2.0 and 2.0–2.5. Each cross point represents a single time of observation. In consideration of the validity of the derived parameters, only the cases with $R^2 > 0.4$ in both the two L shell regions are used. In this figure, most cross points are near the diagonal which suggests that the ϕ_0 are nearly equal between the two L shell regions. Some points are near the left upper corner and right bottom corner, which is caused by the periodicity of the sinusoidal function. The result shown in Figure 6 is consistent with the vertical patterns in the $L - f_d$ spectrogram presented in the case study.

For the sake of statistically exploring the evolutionary features of zebra stripes, we use a similar method as in section 2.3 to analyze all continuous cases. First, we pick single observations by the following criteria: (1) R^2 in both the L shell regions 1.5–2.0 and 2.0–2.5 are larger than 0.4, and (2) the difference of the evolution time T between the L shell regions 1.5–2.0 and 2.0–2.5 is no larger than 1 h. Next, for each case we define the evolution time as the average T of L shell regions 1.5–2.0 and 2.0–2.5. Then, we sort all cases by the observation time UT (when satellite arrives at $L = 2$). Finally, the ΔUT and ΔT of all pairs of adjacent cases are calculated, and their comparisons are shown in Figure 7.

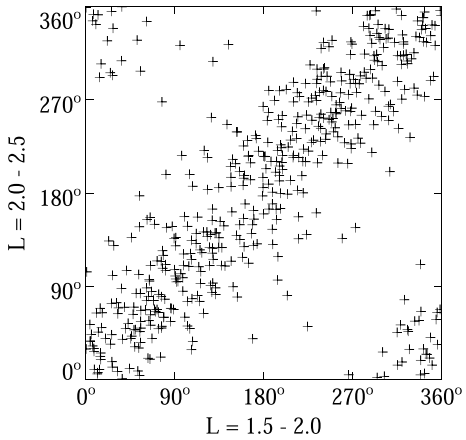

Figure 6. The relationship between phase angles of zebra stripes in L shell region 1.5–2.0 and 2.0–2.5. Each cross point represents one single observation with $R^2 > 0.4$ in both the L shell region 1.5–2.0 and 2.0–2.5.

In Figure 7, one may find that there are a large number of points located at $\Delta UT \approx 1$ h, which is caused by the time separation of two continuous observations of one Van Allen Probe near its perigee. More interestingly, a majority of points are near the diagonal which represents $\Delta T = \Delta UT$. This result is consistent with the evolution features presented in case study; the variation of the evolution time are approximately the same as that of real time.

3. Interpretation and Discussion

3.1. Zebra Stripes Formation Under the Single Monochromatic Azimuthal Electric Field

In section 2 we have shown that the zebra stripes become denser as time progresses in observation.

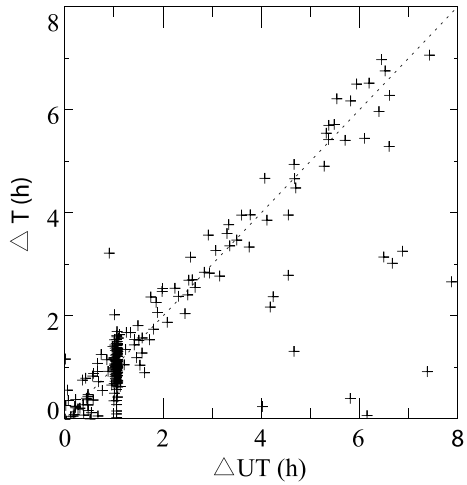

Figure 7. The relationship between ΔT and ΔUT. Each cross point represents parameters derived from one couple of continuous observations with $R^2 > 0.4$. The dotted line represent $\Delta T = \Delta UT$.

This evolutionary feature clearly contradicts the resonance mechanism, which will generate static stripes. A possible solution is from *Ukhorskiy et al.* [2014], who used a test-particle model to show the evolutionary stripes can be produced under the single monochromatic electric field. Now we start from a more general electric field model which is a generalization of the electric field model used in *Ukhorskiy et al.* [2014] to analytically show how zebra stripes form. By comparing the analytic model results with comprehensive Van Allen Probe observations, we could understand the generation and evolution of the zebra stripes in a better way.

In this model, we assume that when $t = 0$, the electron distribution is undisturbed and depends solely on L shell and energy. The electric field is a single monochromatic azimuthal electric field given by

$$E_\phi = E_0 \cos(\omega t - m\varphi + \phi_0) \tag{4}$$

where E_0, ω, m, and ϕ_0 are the amplitude, angular frequency, azimuthal wave number, and initial phase angle of the monochromatic electric field, respectively, and the φ is the azimuthal coordinate. It is noted that static electric fields ($\omega = 0$), the solution in *Ukhorskiy et al.* [2014] ($m = 1$), and ULF waves can be represented by this electric field model. According to Liouville's theorem, the electron's phase space density is constant along the electron trajectory. For equatorially mirroring electrons,

$$f(\mu, L', \varphi'; t') = f_0(\mu_0, L_0) \tag{5}$$

where μ, L', and φ' are the parameters of the electron at time t', μ_0 and L_0 are the magnetic moment and L shell of the electron at time 0, and f_0 is the electron's initial phase space density. Due to the conservation of the first adiabatic invariant we have $\mu_0 = \mu$. By using Taylor expansion, the phase space density at time t' can be expressed as

$$f(\mu, L', \varphi'; t') = f_0(\mu, L_0) \approx f_0(\mu, L') + \left.\frac{\partial f_0}{\partial L}\right|_\mu (L_0 - L') \tag{6}$$

For nonresonant electrons ($\omega \neq m\omega_d$), the variation of the L shell can be expressed as (the detailed derivation is presented in the Appendix):

$$L_0 - L' \approx -\frac{L'^3 E_0}{B_0 R_E(\omega - m\omega_d)}[-\sin(-m\varphi' + \omega t' + \phi_0) + \sin(m\omega_d t' - m\varphi' + \phi_0)] \tag{7}$$

At time t', $-\sin(-m\varphi' + \omega t' + \phi_0)$ is a constant for all electrons, and $\sin(m\omega_d t' - m\varphi' + \phi_0)$ is a sine-like function of ω_d. Therefore, the disturbed phase space density can be arranged as a sinusoidal function of ω_d. The peak and valley values appear at the energies satisfying $m\omega_d t' - m\varphi' + \phi_0 = \frac{\pi}{2} + n\pi$. It is obvious that in any given ω_d range, the number of peaks and valleys increases with increasing time. The analytical results are consistent with the observation features presented in section 2. The evolution feature $\Delta T = \Delta UT$ obtained in Figures 4 and 7 indicates that $m = 1$. Moreover, Formulas (6) and (7) indicates the amplitude of the disturbed phase space density depends on both phase space density gradient $\left.\frac{\partial f_0}{\partial L}\right|_\mu$ and amplitude of the electric field. It is noted that the sine-like patterns remain even if $\omega = 0$. In other words, not only periodic electric fields but also static electric fields can produce zebra stripes.

To understand these analytical results, we illustrate in Figure 8 the generation of zebra stripes under a simple situation with $\omega = 0$. When a uniform duskward electric field is applied at epoch zero, the electron drift motion will deviate from circular orbits. The drift paths of the electrons reach the innermost point in the dawnside,

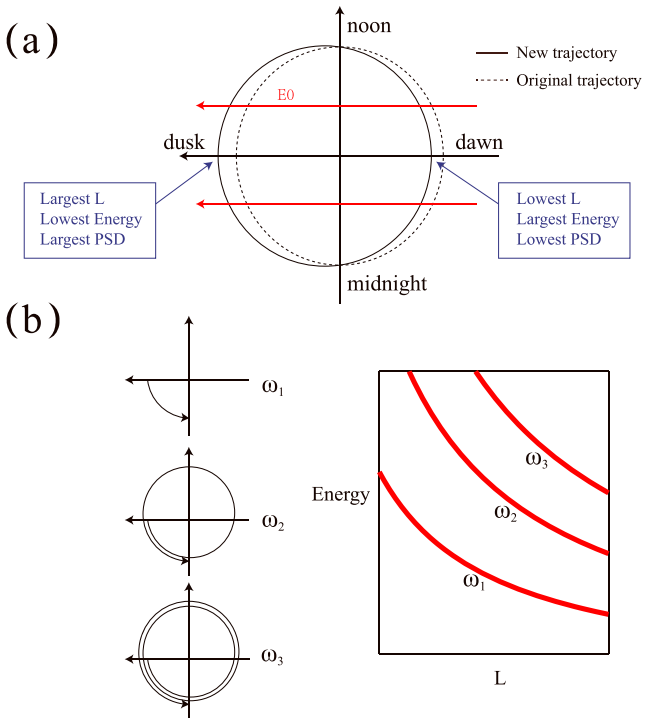

Figure 8. Illustration of the formation of zebra stripes under a static duskward electric field. (a) The drift path of electrons under an uniform static electric field and the phase space density distribution of electrons with a given μ in this drift path at the initial state. (b) Multiple stripes in the electron spectrogram and corresponding electron trajectories.

while the paths reach the outermost point in the duskside. In other words, two electrons captured at different times by the same satellite with the same energy used to have different energies and different L shells at epoch zero and thus have different phase space densities. At this fixed location, the peaks and valleys of the electron distributions will appear periodically due to their drift motion around the Earth: the peak/valley fluxes correspond to electrons launched from the duskside/dawnside sectors at epoch zero.

Although the observations are finely explained by the simple model described above, the real situation can be different from it. The long-lasting single monochromatic azimuthal electric fields are not common in the magnetosphere. Here we consider the electric field lasts until $t = t_E$. Before t_E, the electron distribution evolves following the above model. At time $t' > t_E$, the electric field disappears, but the disturbed electron distribution continues to evolve due to the drift motion. According to the results presented in the Appendix, the disturbed phase space density is arranged as a superposition of two sinusoidal functions of ω_d with frequencies mt' and $m(t' - t_E)$, respectively. Thus, the patterns in the electron spectrogram will be more complicated. However, when $t' \gg t_E$, the variation of L shell can be approximated by a sinusoidal function of ω_d with a slowly changing amplitude and a frequency mt' (see Appendix for details). Then the disturbed phase space density will show similar characteristics as those under the long-lasting electric field discussed above. The condition $t_E \ll t'$ can be easily satisfied by electric fields in the magnetosphere, e.g., a pulsed electric field. In this way, when an azimuthal electric field is established, the zebra stripes in the electron spectrogram start to evolve. After the electric field disappear, the zebra stripes may continue to evolve and therefore become an ubiquitous feature of electrons in the inner radiation belt until another electric field pulse appear to restart the process. However, we should point out that when t_E is very small, the electric field cannot change the energy of electrons obviously before it disappear and no notable zebra stripes can be produced.

3.2. On the Origin of the Electric Field in the Inner Radiation Belt

Quantitative analysis based on Van Allan Probe observations and analytic derivation have shown that zebra stripes can be interpreted as a result of a single azimuthal monochromatic or static electric field. However, the origin of the electric field inside $L = 3$ is still an open question. Based on our analytic model in the previous section, either a static electric field or even transient electric field could produce the observed zebra stripes.

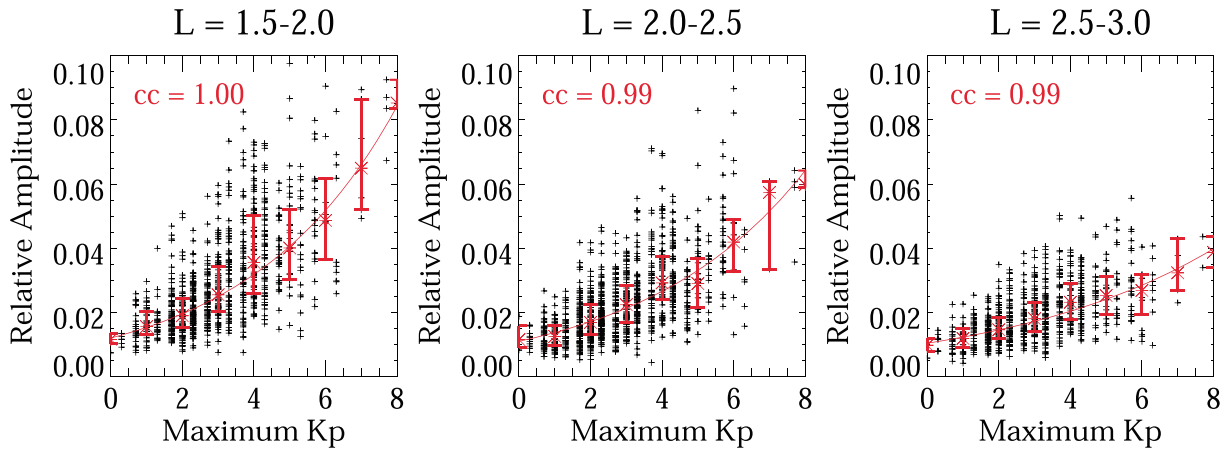

Figure 9. The relationship between the relative amplitude of zebra stripes *A* and maximum *Kp* index in 12 h interval before observation. (left to right) The results in three L shell regions (1.5–2.0, 2.0–2.5, and 2.5–3.0), respectively. Each black cross point represents parameters derived from one single observation with $R^2 > 0.4$. The red star points represent the median values of *A*, and the error bars show the lower and upper quartiles in each *Kp* bin. The red line denotes the linear fit to median value of $\log_{10}A$ and maximum *Kp*, and the parameter cc represents the linear correlation coefficient.

Thus, the convective electric field which generally satisfies $m = 1$ can be another possible driving source for the observed zebra stripes. Due to the interaction between the solar wind and the Earth's magnetic field, the large-scale dawn-to-dusk convection electric field may be set up in the inner magnetosphere. Nevertheless, curvature and gradient drifts cause electrons to drift eastward and ions to drift westward, leading to a polarization electric field pointing from dusk to dawn that shields the inner part of the magnetosphere from the convection electric field [e.g., *Wolf et al.*, 2007]. The rapid changes in the magnetospheric convection can lead to the penetration of the electric field in the inner magnetosphere and low-latitude ionosphere on the basis of undershielding [*Vasyliunas*, 1972] or overshielding [*Kelley et al.*, 1979] mechanism.

Various aspects of the penetration of convection electric field have been studied. Early simulations by *Jaggi and Wolf* [1973] indicated that significant undershielding persisted for about 10 min, and it took about 2 h for complete shielding to occur. However, both recent simulations [*Garner et al.*, 2004] and observations [*Huang et al.*, 2005] suggested that the shielding was not effective for many hours during the storm main phase. Direct observations from Combined Release and Radiation Effects Satellite (CRRES) [*Rowland and Wygant*, 1998] and from Time History of Events and Macroscale Interactions during Substorms (THEMIS) missions [*Califf et al.*, 2014] have also shown that strong electric fields occur inside $L = 3$ during the most active times. The observations indicate that the polarization electric field cannot always shield the near-Earth convection electric field. Especially during geomagnetic storms, strong electric field will penetrate into the inner radiation belt region. Energetic electrons are then influenced by this "penetrated" electric field to generate the zebra stripes.

Since the intensity of this electric field is related to the geomagnetic activities, the amplitude *A* (if $R^2 > 0.4$) of zebra stripes should show correlation with geomagnetic activities if this mechanism is valid. Therefore, we examine the relationship between amplitude *A* and geomagnetic index *Kp*. For each single case, the maximum *Kp* value in the 12 h interval before the observation time is taken as the representative value of the corresponding geomagnetic activity. The result is presented in Figure 9. Figures 9 (left) to 9 (right) show the results in three L shell regions (1.5–2.0, 2.0–2.5, and 2.5–3.0), respectively. This figure shows a good positive correlation between *A* and *Kp* which indicates that the source of zebra stripes is related to geomagnetic activities. The large-scale convection electric field which has not been fully shielded is possibly responsible for the unexpected phenomenon in the inner radiation belt. It should be noted that our result presented here does not exclude the possibility of the rotation mechanism to generate the zebra stripes as suggested by *Ukhorskiy et al.* [2014]. Further, we also fit the median values of *A* in each *Kp* bin and corresponding *Kp* values by the formula $\log_{10}A =$

Table 1. Best Fit Result of *A* and Maximum *Kp* Index

L shell Region	a	b	cc
1.5–2.0	−1.921	0.106	1.00
2.0–2.5	−1.959	0.096	0.99
2.5–3.0	−1.984	0.073	0.99

$a + b \cdot Kp$ as shown in Figure 9. The best fit parameters a and b are presented in Table 1. The linear correlation coefficient is very high (larger than 0.99) in all the three L shell regions. Also, this formula can provide a prediction of the amplitude of zebra stripes and may be further used to estimate the intensity of electric field in the inner radiation belt.

4. Conclusion

In this paper, we have studied the zebra stripes of the electron spectrogram inside $L = 3$. Through case study and statistical analysis of a continuous 1 year interval of the Van Allen Probes measurements, we have revealed the quantitative features of this structure and its evolution. The main results can be summarized as follows:

1. Both case study and statistical study have shown that zebra stripes of the electron spectrogram are evenly spaced patterns in the drift frequency coordinate. The detrended logarithmic fluxes in each L shell region can be described as a sinusoidal function of drift frequency $p = A \sin(2\pi T f_d - \phi_0)$.
2. Zebra stripes follows the equation $\Delta T = \Delta UT$. Here the UT is the observation time of the zebra stripes, and T is a fitted parameter which represents the reciprocal of the gap between two adjacent peaks in the drift frequency coordinate.
3. An analytic model has been developed to generalize the test particle model in *Ukhorskiy et al.* [2014]. The analytic model presented in this paper reveals that the structural and evolutionary features of zebra stripes can be explained quantitatively by considering the trajectory of the electrons under a single monochromatic electric field. Especially, the analytic model reveals that even static electric field and transient electric field can also produce zebra stripes phenomena in the inner magnetosphere.
4. It is found that the strength of the zebra stripes have a good positive correlation with the Kp index. Also, it is suggested that the large-scale penetrated convection electric field can drive zebra stripes of energetic particle in the inner magnetosphere as well.

Appendix A: Electron Trajectory Under the Single Monochromatic Azimuthal Electric Field

Here we give the analytical derivation of the electron trajectory under the single azimuthal monochromatic electric field. We assume that the electron drift frequency is constant during their drift motion. Only equatorially mirroring electrons are considered. The electric field is given by

$$E_\phi = E_0 \cos(\omega t - m\varphi + \phi_0) \tag{A1}$$

where E_0, ω, m, and ϕ_0 are the amplitude, angular frequency, azimuthal wave number, and initial phase angle of the monochromatic electric field, respectively, and the φ is the azimuthal coordinate of the electron. The drift angular velocity of electrons in the dipole field can be given by

$$\omega_d = \frac{3\mu}{\gamma e} \frac{1}{(R_E L)^2} \tag{A2}$$

where μ is the magnetic moment (constant of motion, as long as ω is much smaller than the electron angular gyrofrequency). It is noted that when $\omega = m\omega_d$, the drift resonance between electrons and waves will take place [*Southwood and Kivelson* 1981]. In this paper, we do not consider the resonant electrons. The $\omega \neq m\omega_d$ is acquiescent in the following derivations. The equation of electron motion can thus be given by

$$\begin{cases} \dot{\varphi} = \omega_d \\ \dot{L} = -\frac{E_0 L^3}{B_0 R_E} \cos(\omega t - m\varphi + \phi_0) \end{cases} \tag{A3}$$

For the electrons launched from (L', φ') at time t' with drift angular velocity ω_d, their trajectory can thus be obtained:

$$\frac{1}{L^2} = \frac{1}{L'^2} + \frac{2E_0}{B_0 R_E(\omega - m\omega_d)} \left\{ \sin\left[(\omega - m\omega_d)t + m\omega_d t' - m\varphi' + \phi_0\right] - \sin(\omega t' - m\varphi' + \phi_0) \right\} \tag{A4}$$

Therefore, the initial location L_0, which refers to the L shell of the electrons at $t = 0$, can be given by

$$\frac{1}{L_0^2} = \frac{1}{L'^2} + \frac{2E_0}{B_0 R_E(\omega - m\omega_d)} \left[\sin(m\omega_d t' - m\varphi' + \phi_0) - \sin(\omega t' - m\varphi' + \phi_0) \right] \tag{A5}$$

Treating $L_0 - L'$ as a small parameter, the variation of the L shell of the electrons can be written as

$$L_0 - L' \approx -\frac{L'^3 E_0}{B_0 R_E(\omega - m\omega_d)} \left[\sin(m\omega_d t' - m\varphi' + \phi_0) - \sin(\omega t' - m\varphi' + \phi_0)\right] \tag{A6}$$

To understand this formula, we can consider the drift paths of electrons in the wave reference frame, noting that electrons drift inward and outward under westward and eastward electric field, respectively. When they drift in the single monochromatic electric field, they periodically experience westward and eastward electric field. Thus, the variation of L shell of electrons is also periodical and can be represented as a sinusoidal function.

If the electric field lasts until t_E, the electrons would then drift along circular orbits and keep energy unchanged after t_E. The initial location L_0 of the electrons locate at position (L', φ') at time $t' > t_E$ depends on their locations $(L', \varphi' - (t' - t_E)\omega_d)$ at time t_E. Thus, we can obtain the initial location of the electrons at time t':

$$L_0 - L' \approx -\frac{L_0'^3 E_0}{B_0 R_E(\omega - m\omega_d)} \{\sin(m\omega_d t' - m\varphi' + \phi_0) - \sin[m(t' - t_E)\omega_d - m\varphi' + \phi_0 + \omega t_E]\} \tag{A7}$$

which is a superposition of two sinusoidal functions of ω_d with frequencies mt' and $m(t' - t_E)$, respectively. The above expression can be also written as

$$L_0 - L' \approx -\frac{2L'^3 E_0}{B_0 R_E(\omega - m\omega_d)} \cos\left[m\left(t' - \frac{t_E}{2}\right)\omega_d - m\varphi' + \phi_0 + \frac{\omega t_E}{2}\right] \sin\left(m\frac{t_E}{2}\omega_d - \frac{\omega}{2}t_E\right) \tag{A8}$$

which suggests that the variation of L shell can be regarded as a sinusoidal function of ω_d with the frequency mt' and a slowly changing amplitude when $t_E \ll t'$. Then the variation of L shell for electrons satisfy similar characteristics under this short-lasting electric field (e.g., a pulsed electric field) as those under a long-lasting electric field. It is noted that when t_E is very small, the amplitude is negligible since $\sin(m\frac{t_E}{2}\omega_d - \frac{\omega}{2}t_E) \approx 0$.

Acknowledgments
This work was supported by National Natural Science Foundation of China (41421003) and Major Project of Chinese National Programs for Fundamental Research and Development (2012CB825603). The RBSPICE data used in this study are available from rbspice.ftecs.com.

References

Califf, S., et al. (2014), THEMIS measurements of quasi-static electric fields in the inner magnetosphere, *J. Geophys. Res. Space Physics*, *119*, 9939–9951, doi:10.1002/2014JA020360.

Cladis, J. (1966), Resonance acceleration of particles in the inner radiation belt, in *Radiation Trapped in the Earth's Magnetic Field*, edited by B. M. McCormac, 112 pp., Springer, New York.

Datlowe, D. W., W. L. Imhof, E. E. Gaines, and H. D. Voss (1985), Multiple peaks in the spectrum of inner belt electrons, *J. Geophys. Res.*, *90*(A9), 8333–8342, doi:10.1029/JA090iA09p08333.

Garner, T. W., R. A. Wolf, R. W. Spiro, W. J. Burke, B. G. Fejer, S. Sazykin, J. L. Roeder, and M. R. Hairston (2004), Magnetospheric electric fields and plasma sheet injection to low L-shells during the 4–5 June 1991 magnetic storm: Comparison between the Rice Convection Model and observations, *J. Geophys. Res.*, *109*, A02214, doi:10.1029/2003JA010208.

Huang, C., J. C. Foster, and andM. C. Kelley (2005), Long-duration penetration of the interplanetary electric field to the low-latitude ionosphere during the main phase of magnetic storms, *J. Geophys. Res.*, *110*, A11309, doi:10.1029/2005JA011202.

Imhof, W. L., and R. V. Smith (1966), Low altitude measurements of trapped electrons, in *Radiation Trapped in the Earth's Magnetic Field*, vol. 100, edited by B. M. McCormac, Springer, New York.

Imhof, W. L., E. E. Gaines, and J. B. Reagan (1981), High-resolution spectral features observed in the inner radiation belt trapped electron population, *J. Geophys. Res.*, *86*, 2341–2347, doi:10.1029/JA086iA04p02341.

Jaggi, R. K., and R. A. Wolf (1973), Self-consistent calculation of the motion of a sheet of ions in the magnetosphere, *J. Geophys. Res.*, *78*, 2852–2866, doi:10.1029/JA078i016p02852.

Kelley, M. C., B. G. Fejer, and C. A. Gonzales (1979), An explanation for anomalous ionospheric electric fields associated with a northward turning of the interplanetary magnetic field, *Geophys. Res. Lett.*, *6*, 301–304, doi:10.1029/GL006i004p00301.

Mauk, B. H., N. J. Fox, S. G. Kanekal, R. L. Kessel, D. G. Sibeck, and A. Ukhorskiy (2012), Science objectives and rationale for the Radiation Belt Storm Probes mission, *Space Sci. Rev.*, *179*, 3–27, doi:10.1007/s11214-012-9908-y.

Mitchell, D. G., et al. (2013), Radiation Belt Storm Probes Ion Composition Experiment (RBSPICE), *Space Sci. Rev.*, *179*, 263–308, doi:10.1007/s11214-013-9965-x.

Roederer, J. G. (1970), *Dynamics of Geomagnetically Trapped Radiation*, Springer, New York.

Rowland, D. E., and J. R. Wygant (1998), Dependence of the large-scale, inner magnetospheric electric field on geo-magnetic activity, *J. Geophys. Res.*, *103*, 14,959–14,964, doi:10.1029/97JA03524.

Sauvaud, J.-A., M. Walt, D. Delcourt, C. Benoist, E. Penou, Y. Chen, and C. T. Russell (2013), Inner radiation belt particle acceleration and energy structuring by drift resonance with ULF waves during geomagnetic storms, *J. Geophys. Res. Space Physics*, *118*, 1723–1736, doi:10.1002/jgra.50125.

Southwood, D. J., and M. G. Kivelson (1981), Charged particle behavior in low-frequency geomagnetic pulsations: 1. Transverse waves, *J. Geophys. Res.*, *86*, 5643–5655, doi:10.1029/JA086iA07p05643.

Tsyganenko, N. A., and M. I. Sitnov (2005), Modeling the dynamics of the inner magnetosphere during strong geomagnetic storms, *J. Geophys. Res.*, *110*, A03208, doi:10.1029/2004JA010798.

Ukhorskiy, A. Y., M. I. Sitnov, D. G. Mitchell, K. Takahashi, L. J. Lanzerotti, and B. H. Mauk (2014), Rotationally driven 'zebra stripes' in Earth's inner radiation belt, *Nature*, *507*, 338–340, doi:10.1038/nature13046.

Vasyliunas, V. M. (1972), The interrelationship of magnetospheric processes, in *The Earth's Magnetospheric Processes*, pp. 29–38, Springer, D. Reidel Dordrecht, Netherlands.

Wolf, R. A., R. W. Spiro, S. Sazykin, and F. R. Toffoletto (2007), How the Earth's inner magnetosphere works: An evolving picture, *J. Atmos. Sol. Terr. Phys.*, *69*, 288–302.